Distinct Element Method Simulations of Rock-Socketed Piles: Estimation of Side Shear Resistance Considering Socket Roughness

J. G. Gutiérrez-Ch[1], S. Melentijevic[2], S. Senent[3], and R. Jimenez[4]

ABSTRACT

Rock-socketed piles are foundation elements designed to transmit large concentrated loads to stronger materials located at greater depths. The rock-socket side shear resistance is commonly estimated using empirical criteria, as a percentage of the rock or concrete uniaxial compressive strength. However, this approach neglects the influence of other important aspects, such as the roughness of the pile-socket interface. In this work, numerical discrete element models of rock-socketed piles with different degrees of socket roughness are employed to estimate the influence of the socket roughness on the load-settlement response, and on the side shear resistance. The numerical simulation results are compared with predictions obtained using empirical correlations based on load test results and proposed by other authors. Results indicate that the discrete element method is suitable to reproduce rock-socket pile behavior considering socket roughness; they also suggest that sockets drilled with standard tools in soft to medium rock tend to be relatively smooth, unless artificially roughened with special tools; and that damage to the interface asperities becomes more relevant after socket settlement of about 1% of the socket diameter, especially for rougher piles.

Keywords Rock-socketed piles, side shear resistance, socket roughness, UCS, DEM.

1 Introduction

The design of axially loaded rock-socketed piles aims to transfer the structural load to a stronger and deeper foundation material. Although the load transfer mechanism usually combines base and side resistances, the contribution of side shear

resistance is often crucial, as it mobilizes at much lower strains (or pile settlements) than base resistance. There are also situations in which pile base resistance cannot be relied upon, due to lack of quality of the pile base (e.g., debris accumulated at bottom, or rock with cavities) (Seidel and Collingwood 2001).

Fundamentals of shear strength of interfaces have been investigated through laboratory tests that lead to the development of analytical and empirical models to predict the shear strength of rock-rock interfaces (Patton 1966; Barton and Choubey 1977) or of rock-concrete interfaces (Kodikara and Johnston 1994). Other models to study the shear behavior of geotechnical interfaces considering their roughness (Barton et al. 1985), or the influence of anisotropy and grain size of materials involved in such interfaces (Kishida and Uesugi 1987; Wang et al. 2007) have also been proposed. However, the side shear resistance of rock-socketed piles is usually estimated using recommendations from codes and standards, or using local knowledge obtained from full-scale static load tests performed in similar ground (Seidel and Collingwood 2001); empirical correlations to estimate it as a function of the uniaxial compressive strength (UCS or σ_c) are also common (Rezazadeh and Eslani 2017) (Section 3.1.3 further discusses some of the most common ones). However, in agreement with the conclusions of O'Neill et al. (1996) after their analysis of 245 load tests in different materials, other parameters in addition to the UCS are required for an improved estimation of the side shear resistance. As likely candidates to be considered, the main factors affecting the side shear resistance are: the construction method and drilling tools used (Nam and Vipulanandan 2008; O'Neill et al.1996; Ng et al. 2001), the type and quality of the rock mass (Haberfield

2013; Melentijevic and Olalla 2014), the depth and diameter of the socket (Seidel and Haberfield 1995; Seol and Jeong 2007), the residual drilling fluid coating the socket walls and the thickness of smear zone (Williams and Pells 1981; Haberfield 2013), and the initial normal stress and roughness at the pile-rock interface (Horvath and Kenney 1979; Pells et al. 1980; Horvath et al. 1983; Seidel and Collingwood 2001; Seol et al. 2009).

This paper studies the influence of roughness at the socket's concrete-rock interface, and how it affects rock-socketed piles. This is because (i) full-scale and model pile tests demonstrate that socket roughness has a large influence on the side shear resistance of rock-socketed piles (see Pells et al. 1980; Horvath et al. 1983; Seol and Jeong 2007; Nam and Vipulanandan 2008; Dai et al. 2017); and because, despite its importance, (ii) socket roughness is not often considered in current design practice. To that end, the roughness factor (RF) defined by Horvath at al. (1983) is used as a quantitative measure of roughness, and to investigate its influence on pile performance. In particular, this paper applies the Distinct Element Method (DEM) to model rock-socketed piles, and analyzes the effect of socket roughness on their side shear behavior.

2 Numerical model to simulate rock-socketed piles in DEM^{3D}

2.1 Introduction and fundamentals

Particle Flow Code (PFC) (Itasca Consulting Group Inc 2014) is the commercial software with a DEM implementation employed in this paper. In a DEM model, the displacements and interactions of systems composed by rigid and finite-sized

particles –spherical in PFC^{3D}, see **Fig. 1**(a)– can be simulated. Mechanical interactions are created or destroyed by the contact-detection algorithm whenever bodies are sufficiently close or separated. The system evolution is computed through explicit dynamic simulation schemes that apply Newton's second law to the particles, and that consider a force-displacement law at the contacts (Itasca Consulting Group Inc 2014). PFC provides a Bonded-Particle Model (BPM) to simulate cohesive material (e.g., concrete or rock) with several possible contact models (Potyondy 2015), as well as "interfaces" among materials to characterize their behavior when they are in contact. In this work, the Flat-Joint Contact Model (FJCM) is employed to simulate the pile and rock bodies, whereas the Smooth-Joint Contact Model (SJCM) is employed to reproduce the behavior at the rock-concrete interface.

The FJCM simulates the contact between particles in the BPM using locally notional (bonded or unbonded) surfaces (see **Fig. 1**(a)), which are discretized into elements (Potyondy 2012). The SJCM simulates the macroscopic behavior of a bonded or unbonded interface formed by several particles, in which particles can overlap or slide past each other, to avoid moving around one another (see **Fig. 1**(b)). In both models, the behavior of bonded interfaces is linear elastic until the bond strength is reached and the bond breaks, making the interface unbonded (Itasca Consulting Group Inc 2014). Unbonded interfaces have a linear, elastic and frictional behavior in which the slip is simulated by a Coulomb limit on the shear force. For additional details, see Potyondy (2015), Ivars et al. (2008), and Itasca Consulting Group Inc (2014).

In this work, DEM numerical models are used to calculate the side shear resistance of rock-socketed piles with different levels of socket roughness. To that end, calibrating the micromechanical parameters that control the macroscopic behavior of the rock and concrete, or of the rock-concrete interface, is needed first. (Experimental data published by Gu et al. (2003) –about the shear behavior of sandstone-concrete interfaces– and by Gutiérrez (2013) –about gneiss-concrete interfaces– are used.) Finally, the procedure to generate samples for numerical testing of rock-socketed piles is presented.

2.2 Calibration of micromechanical parameters

The calibration process has two steps: first, the FJCM parameters are calibrated, using one UCS test as reference; then, the SJCM parameters are calibrated, using one direct shear test as reference. Such calibration of micromechanical parameters is conducted in 2D. The main reason for this is computational efficiency: 2D models are much faster than 3D models, and many model runs are required for the calibration. But, in agreement with previous research (see e.g., Ding et al., 2014), results also indicate that the influence of the 2D vs. 3D calibration on the macroscopic behavior of such tests is small; and we have also noted that the behavior at the rock socket interface is similar to a (2D) direct shear test, with radial horizontal displacements of particles and negligible particle rotations at the interface. This suggests that the difference of pile behavior due to a 2D vs 3D calibration are probably small and probably do not justify the large increase of computational cost associated to a 3D calibration.

2.2.1 Calibration of the Flat-Joint Contact Model

To calibrate the micromechanical parameters of the FJCM employed for intact (rock or concrete) materials, the uniaxial compressive strength (UCS) test is commonly used to compare numerical and laboratory tests results. The procedure is iterative and starts matching the macroscopic Poisson's ratio (ν), which mainly depends on the particle and flat-joint normal-to-shear stiffness ratio (k^* and $\overline{k^*}$); next, the macroscopic Young's modulus (E), is calibrated modifying the particles and flat-joint effective modulus (E^* and $\overline{E^*}$); finally, the UCS (σ_c) is adjusted by tuning the cohesion (c) and tensile strength (σ_t) of the flat-joint. There are others parameters of the FJCM –such as the friction angle of the material (ϕ), the bonded fraction ($\phi_B = \eta_B/\eta_{FJ}$, where η_B and η_{FJ} are the number of bonded and total flat-joint contacts, respectively), the initial surface gap (g_o), and the gapped fraction ($\phi_G = \eta_G/\eta_{FJ}$, where η_G is the number of gapped contacts: i.e., contacts between particles with a separation greater than g_o, so there are not interactions between particles),– that could also influence the behavior of the material, but they are not considered in the calibration conducted herein (for details, see Gutiérrez-Ch et al. 2018).

Table 1 lists the micromechanical properties obtained with numerical samples of sandstone (types S2 and S3), gneiss and concrete (types C1 and C2) after the calibration process. **Table 2** compares the macroscopic UCS test results –σ_c, E, ν– obtained experimentally by Gutiérrez (2013) (for gneiss and C2-concrete) and by Gu et al. (2003) (for S2- and S3-sandstone and C1-concrete) with those simulated with DEM^{2D} employing the parameters listed in **Table 1**. It can be observed that (i) the average values calculated with the DEM^{2D} numerical models agree well with the

laboratory results, and (ii) that the standard deviation of results obtained in experimental tests (when reported) is greater for rock samples than for concrete. This is probably due to the presence of minor defects in rock samples –e.g., weak planes, microcracks, etc.– which are probably not so common in a manufactured material such as concrete. Note also that the DEM results present similar standard deviation for rock and concrete samples, as the sample generation algorithm is equivalent for both.

2.2.2 Calibration of the Smooth-Joint Contact Model

The SJCM parameters –i.e., the smooth-joint's normal and shear stiffness ($k_{n\,SJ}$ and $k_{s\,SJ}$); and its coefficient of friction ($\mu_{\,SJ}$)– are calibrated comparing numerical and experimental results of direct shear tests on unbonded (i.e., with $c = 0$) rock-concrete planar interfaces under different normal stresses. To that end, numerical specimens are generated first, using the Shear Box Genesis (SBG) method proposed by Bahaaddini et al. (2013). **Fig. 2**(a) shows an example of one of such specimens formed by an interface between concrete-C1 and sandstone-S2 (the interface is modelled using the smooth-joint contact model, and the interactions between particles of each body are modelled using the flat-joint contact model with the micro-mechanical properties listed in **Table 1**).

Then, the numerical joint normal stiffness ($K_{n\,DEM}$) is calibrated against the laboratory normal stiffness ($K_{n\,lab}$) through a normal deformability test on planar joints, in which the value of $k_{n\,SJ}$ is adjusted. Finally, the joint shear stiffness ($K_{s\,DEM}$) and the coefficient of friction (μ_{DEM}) are calibrated by trial and error, adjusting the value of $k_{s\,SJ}$ and $\mu_{\,SJ}$ to reproduce the behavior of laboratory shear tests (i.e., the shear

stiffness, $K_{s\,lab}$, and the peak shear strength measured in the laboratory). The DEM^{2D} results of direct shear tests on unbonded sandstone (S2)-concrete (C1) planar interfaces are presented in **Fig. 2**(b), and the calibrated SJCM parameters are listed in **Table 3**. Results show that DEM^{2D} models can reproduce the behavior of concrete-rock interfaces, so that they agree well with experimental results reported by Gu et al. (2003) and by Gutiérrez (2013) (see **Table 4Table 3**). For additional details about calibration, see also Bahaaddini et al. (2013) and Gutiérrez-Ch et al. (2018).

2.3 Generation of samples to simulate rock-socketed piles

Fig. 3 presents an idealized sub-surface profile of a rock socket, and the associated DEM^{3D} model developed to represent it. The methodology to simulate rock-socketed piles in this DEM^{3D} model can be summarized as follows:

2.3.1 Initial particle assembly of rock and pile bodies

The 3D model of the rock-socketed pile consists of several frictionless walls to avoid shear forces from developing at ball-wall boundary contacts and to reduce boundary effects. Such walls are filled with two assemblies of randomly placed particles that constitute the concrete pile and the rock around it (**Fig. 4**(a)). The normal stiffness of the walls is set to be larger than the average particle normal stiffness to ensure that particle–wall overlaps remain small. Particle sizes at the different zones considered follow a uniform distribution of radii between R_{min} and R_{max} bounds chosen after a sensitivity analysis (not reproduced herein) that indicated that socket behavior is not affected by particles whose size (at zone 1) are within this interval (see **Table 5**).

To optimize the computational cost, (i) the rock body was discretized into three zones, defined as a function of the nominal socket radius, R, and with the smallest particles being positioned adjacent to the pile-rock interface (zone 1) (see Fig. 4(a)); and (ii) a portion of only $1/8$ of the pile cross-section (or of a 45-degree angle) was modeled, instead of the whole cross section (see Fig. 4(b)). The base was made void because only the pile shaft behavior is analyzed; note also that the particles have a strong cohesion, which prevents them from falling into the void. The nominal socket radius (R) and the nominal socket length (L) are 0.4 m and 0.8 m, respectively, in all analyses presented herein.

2.3.2 Application of an isotropic initial stress

After the initial assembly of particles is created, the "secondary walls" employed to discretize the rock into three zones are removed (see **Fig. 4**(a)). Then, to get a better distribution of contacts and to reduce the locked-in forces, the radii of all particles are iteratively changed until a target isotropic stress ($\sigma_o^c \cong 1\%$ of the uniaxial compressive strength) is reached. To do this, "measurement regions" –spheres in 3D– are installed inside the pile and rock bodies, and the isotropic stress ($\sigma_o = (\sigma_{11} + \sigma_{22} + \sigma_{33})/3$) within each "measurement region" is computed; see **Fig. 4**(c). The process finishes when the normalized difference between the target isotropic stress in all spheres and the specified value of isotropic stress is less than the tolerance (in agreement with Bahaaddini et al. 2013 and Gutiérrez-Ch et al. 2018, the following relation is used $\frac{\sigma_o^c - \sigma_o}{\sigma_o^c} \leq 0.5$).

2.3.3 Elimination of floating particles

"Floating" particles with less than three contacts can appear during the previous step, as illustrated by the red balls shown in **Fig. 4**(d). When this occurs, the radii of floating particles are increased until all particles away from the specimen boundaries have at least three contacts.

2.3.4 Application of Flat-Joint and Smooth-Joint Contact Models

First, flat-joint contacts are installed between particles in each material with a gap lower than g_o (the micromechanical parameters of such flat-joint contacts are listed in **Table 1**). Next, the wall corresponding to the intended contact –the rock-concrete interface– is removed. Finally, particles in contact with the intended rock-concrete surface are identified, and the SJCM is applied to the contacts between balls forming the rock and concrete bodies, employing the micromechanical properties listed in **Table 3**.

Fig. 5(a) shows the model after these contact models are applied; it also shows –using purple arrows that represent the unit normal vectors ($\hat{n}_j$) of the SJCM applied at each contact at the rock-concrete interface (see **Fig. 1**(b))– how the socket roughness affects the orientation of such contacts. To do that, and since the orientations of the interface contacts varies depending on the socket roughness, a FISH function –FISH is an embedded scripting language that enables the user to interact with, and to manipulate, PFC models (Itasca Consulting Group Inc 2014)– was developed to define and update the unit normal vector ($\hat{n}_j$) of the SJCM perpendicular to the rock-concrete interface. Such unit normal vectors have been

plotted in stereographical projections (Ragan 2009) that illustrate the variability of orientations due to roughness, as shown in **Fig. 5**(b).

Fig. 6 illustrates the shapes of the rock-socketed piles considered in this work, and their boundary conditions; it also shows how the DEM^{3D} model of a portion of the rock socket is created, with the corresponding pile self-weight and overburden loads (Q_1 and Q_2, respectively) acting on it. 16 rock-socketed piles (6 on sandstone-S3, 5 on sandstone-S2, and 5 on gneiss) with different degrees of socket roughness were modelled. The RF is employed to quantify roughness; it is defined as (Horvath et al. 1983):

$$RF = \frac{h_m L_t}{RL} \tag{1}$$

where h_m is the average height of asperities, R is the nominal socket radius, L_t is the total travel distance along the socket wall, and L is the nominal socket length (see **Fig. 7**).

According to O'Neill et al. (1996) and Hassan et al. (1997), the socket roughness was simulated using sinusoidal surfaces with amplitudes of 0, 4, 10, 20, 32.5 and 40 mm; and with a wavelength of 250 mm. These values correspond to roughness factors of $RF = 0.000$, $RF = 0.010$, $RF = 0.025$, $RF = 0.050$, $RF = 0.085$, $RF = 0.106$. **Fig. 6**(b) illustrates the roughness profiles associated to each RF, using radial cross-sections of the corresponding DEM^{3D} models. Also remember that (i) the micro-properties used for the FJCM and the SJCM are listed in **Table 1** and **Table 3** (note that, although the calibrated SJCM parameters used in DEM^{3D} models originate from DEM^{2D} models, its expected influence on the obtained results is small,

see e.g., Ding et al., 2014), and (ii) that the particle size distribution (R_{max}/R_{min}) is presented in **Table 5**. The reader should note that a "perfectly smooth" interface with a $RF = 0.000$ might not actually be achievable in practice with any of the usual drilling tools. However, numerical models with $RF = 0.000$ are also considered to provide a lower bound.

2.3.5 Initialization of in situ stress and boundary conditions

The next steps, as shown in **Fig. 6**(a), are to apply a gravity load to induce in situ stresses due to self-weight, and to apply external stresses that represent the overlying loads due to the soil stratum (Q_2) and to the self-weight of the upper portion of the pile (Q_1). To that end, a servo-control mechanism is employed, as it enables one to control the translational velocity of selected walls, so that a desired force can be applied or maintained on them (Itasca Consulting Group Inc 2014). This allows one to model only the rock socket, hence significantly reducing the size of the computational model, and the associated computational cost. Note, therefore, that the analyses herein neglect the elastic shortening of the portion of the pile above the rock socket, as well as the (probably small) side shear resistance developed in it.

To conduct the numerical pile tests, the displacements of the boundary walls or fixed walls shown in **Fig. 6**(a) are restraint, and an axial velocity (V_z) of 0.05 m/s –or low enough to ensure that the rock-concrete specimens remain in quasi-static equilibrium– is applied on the moving wall that represents the rock-socket head. The axial force (P) and the settlement of the socket head (δ) are obtained, respectively, as the force reaction recorded at the wall representing the rock-socket head and as the axial displacements of such wall.

3 Results

3.1.1 Load-settlement response

The load-settlement curves from the DEM^{3D} simulations of six piles socketed into sandstone-S3 (with different roughness profiles) are shown in **Fig. 8**. (Remember that side loads developed along the portion of the pile embedded in soil, as well as its elastic shortening, are neglected, see **Fig. 3**). All analyses were conducted until a limit socket head settlement (δ) of 10% of the socket diameter (0.1*D*) is reached. Results in **Fig. 8** show that socket roughness is an important factor that significantly increases the load capacity and stiffness of rock-socketed piles: for instance, and as shown in **Table 6**, the model with $RF = 0.050$ supported a working load 2.1 times higher than that supported by the model with $RF = 0.025$, for an identical pile head settlement of 0.02*D*. (A similar behavior is also obtained in piles socketed into sandstone-S2 and gneiss). This qualitatively agrees with the results of field tests conducted on sandstone by Pells et al. (1980), in which the "rough" piles supported a higher working load –about 1.2 to 1.7 times higher, depending on the UCS of the rock (sandstone with $\sigma_c = 6 - 40$ MPa)– than the "smooth" piles. Similarly, an influence of RF on the load test results of pile sockets in shale was also observed by Horvath et al. (1983), who reported that the pile with $RF = 0.076$ supported a working load 1.3 times higher than the model with $RF = 0.036$, for a pile head settlement equivalent to 0.02*D*, see **Table 6**.

3.1.2 Average side shear resistance

Considering that DEM^{3D} models are composed by an assembly of particles, and that the pile models considered herein have a void at their base, the average side shear

296 resistance developed along the socket was obtained through an averaging
297 procedure, as:

$$f_{ave} = \frac{\sum F_z}{A} \quad (2)$$

298 where f_{ave} is the average side shear resistance (for a given settlement), $\sum F_z$ is the
299 sum of all vertical components of contact forces acting on all particles at the rock-
300 concrete interface, and A is the nominal side area of the rock-concrete interface.

301 The computed curves relating f_{ave} and δ for rock sockets with different roughness
302 are presented in **Fig. 9**(a) and **Fig. 10**. Results show that the average side shear
303 resistance increases as the roughness of the interface increases; for instance, f_{ave}
304 of the models with $RF = 0.025$ is about 2 times higher than that obtained with $RF =$
305 0.010. This is because the rougher interface (i.e., with higher RF), tends to dilate
306 more and, due to the constraints at the rock socket, which is probably close to a
307 constant normal stiffness (CNS) boundary condition (see Gutierrez-Ch et al. 2018
308 for a discussion), this significantly increases the normal stresses at the rock-socket,
309 hence significantly increasing the side shear resistance of interfaces with higher RF
310 (see e.g., Seol and Jong 2007; Gutierrez-Ch et al. 2018).

311 The analysis of the number of micro-cracks developed at the body of the pile, and at
312 the rock surrounding it, also provides interesting information. **Fig. 9**(b) shows that
313 the number of such microcracks in piles socketed into sandstone-S3 is very small
314 before reaching a settlement of 0.01*D*, and that it increases, with a higher rate for
315 rougher sockets, after such threshold. (Similar results are also obtained in
316 sandstone-S2 and gneiss). This finding is supported by previous works (see e.g.,

317 Bahaaddini et al. 2013; Gutiérrez-Ch et al. 2018), suggesting that models with lower
318 RF values fail through sliding along the rock-concrete interface, whereas the
319 degradation of asperities becomes more relevant for higher RF values (the need to
320 break the asperities is also responsible for the higher side shear resistances
321 developed along rougher interfaces). Note also that the number of cracks (due to
322 shear and tension) is greater in the rock than in the pile. This was expected, as the
323 sandstone rock considered in these models is much weaker than the concrete
324 forming the piles. Results in **Fig. 9**(b) suggest that the criterion of considering a
325 maximum settlement of 0.01*D* under design working loads (see e.g., Whitaker and
326 Cooke 1966; Horvath and Kenney 1979) is probably appropriate to avoid excessive
327 damage of rock-concrete interface of rock socket piles.

328 **Fig. 11** shows the relationship between the roughness of the rock-concrete interface
329 (as defined by the RF roughness factor) and its average side resistance, for two
330 threshold values of pile head displacements. The DEM^{3D} results are computed for
331 socket head settlements of 1% and 2% of the pile diameter, and they suggest that
332 the relationship is approximately linear for lower settlements, for which a significant
333 degradation of the socket interface has not yet occurred. However, the relationship
334 seems to be non-linear for higher settlements, associated to a significantly higher
335 number of cracks (see **Fig. 9**(b)). In agreement with previous research (see e.g., Dai
336 et al. 2017), this suggests that there might be an upper roughness limit, so that the
337 side resistance stops increasing (or increases much slower) when the roughness
338 increases beyond such threshold. In any case, results in **Fig. 11** confirm that socket
339 roughness is an important factor that could be incorporated in the design of rock-

socketed piles. Next, the authors present additional DEM^{3D} analyses, comparing their results with the results of several other methods proposed in the literature, some of which consider the socket roughness for their predictions.

3.1.3 Comparisons with other design methods

This section compares the results of the numerical pile tests conducted with DEM^{3D} –in particular the average side shear resistance for socket head settlements of 0.01*D,* or $f_{ave,0.01D}$– with estimations of other empirical and analytical criteria published in the literature that also used 0.01*D* as a reference settlement to estimate average side shear resistance.

To that end, the range of socket roughness that can be expected in real projects is analyzed first, based on a literature review conducted by the authors. The results of this analysis are compiled in **Table 7**. As it can be observed, and as supported by previous works (see e.g., Collingwood 2000; Seidel and Collingwood 2001), socket roughness is mainly a function of the drilling tools employed and of the type and strength of the rock. In particular, **Table 7** suggests that sockets drilled with standard tools in soft to medium rock tend to be relatively smooth (with height of asperities less than 10 mm), unless the rock is heavily fractured or a special tool is used to increase their roughness.

Empirical criteria that estimate the side shear resistance of the rock socket as a function of the uniaxial compressive strength are employed, as follows:

$$f_{ave,peak}[\mathrm{MPa}] = \alpha \sigma_c[\mathrm{MPa}]^{\beta} \tag{3}$$

where $f_{ave,peak}$ is the average ultimate side shear resistance, σ_c is the intact UCS of the weaker of the materials involved at the shear surface (rock or pile), and α and β are empirical factors that depend on the type of rock, or in some cases on the roughness (Seo et al. 2013). (Other authors –see e.g., Kulkarni and Dewaikar 2016– have also proposed correlations with the UCS of the rock mass; such correlations, however, are not reviewed herein).

Table 8 shows compilation of methods that conform to Equation (3), and that have been proposed in the literature to estimate socket side resistance. (Note that, some of these methods incorporate the influence of roughness, using the roughness classes defined by Pells et al. (1980) that are listed in **Table 9**).

Results computed herein are also compared with the results of other methods proposed in the literature to estimate the average side shear resistance considering the UCS of the material and the socket roughness (see e.g., Pells et al. 1980; Horvath et al. 1983) as well as with the results of the method by Seidel and Collingwood (2001), which considers additional parameters –e.g., the effect of construction method (η_c), the Poisson's ratio (ν), etc.– through a non-dimensional factor called the shaft resistance coefficient (SRC).

Fig. 12 shows the comparison between these analytical and empirical solutions with our DEM^{3D} results; **Fig. 12** compares (i) the average side shear resistance computed with the Sandstone-S3 DEM^{3D} model for a head settlement of $0.01D$, $f_{ave,0.01D}$, and (ii) its predictions computed with the empirical and analytical methods mentioned above. Unless it is specified that the method is valid for certain types of socket only –e.g., smooth or rough–, all the RF values are considered for the DEM^{3D} simulations.

This is why, for methods that not consider socket roughness, $f_{ave,0.01D}$ results are same regardless of RF. Results in **Fig. 12** suggest that, despite the uncertainties involved, the DEM^{3D} model is able to reproduce the overall predictions of the methods analyzed, when an adequate range of roughness (or of RF values) is considered. In that sense, for instance, results with the formulations by Serrano et al. (2015) –which is developed for "smooth" piles– and by Rosenberg and Journeaux (1976) –which employed data of load tests conducted on artificially roughened sockets reported by Matich and Kozicki (1967), as well as sockets constructed in highly fractured rock, which probably produced rough walls– agree quite well with our DEM^{3D} results for $RF = 0.010$ ($h_m = 4$ mm) and for $RF = 0.106$ ($h_m = 40$ mm), respectively; which are therefore within the "smooth" range of real piles or the "rough" range of artificially roughened piles (see **Table 7**).

The methods of Williams et al. (1980) and Horvath and Kenny (1979) also provide $f_{ave,0.01D}$ results that are similar to those computed with DEM^{3D} for relatively smooth sockets (see **Fig. 12**); this agrees with the observation in **Table 7**, as (i) Williams et al. (1980) piles were mainly constructed in a weak mudstone that produced asperities with low height (with $h_m \leq 10$ mm calculated using socket roughness profiles, see Williams 1980), and (ii) Horvath and Kenny (1979) indicate that they worked with "load-test data concerning rock-socketed piers constructed by conventional procedures", and based on the information provided in **Table 7**, this suggests that the average height of asperities is probably less than 10 mm. A similar discussion can be made about the results with the method proposed by Arioglu et al. (2018): although the authors do not report details about the drilling tools

406 employed, the information provided about rock types and rock strengths suggests
407 that average roughness were probably less than 10 mm, since standard drilling tools
408 were used (see **Table 7**).

409 Out of the formulations that specifically consider the socket roughness, the criterion
410 of Rowe and Armitage (1987) –which was proposed using loads test for which socket
411 roughness were measured ($h_m \leq 75$ mm)– provides values similar to the "smoother"
412 DEM^{3D} models (with $RF \leq 0.050$; see **Fig. 12**), whereas numerical results are
413 significantly higher than the predictions of Rowe and Armitage (1987) for rougher
414 sockets. This was also expected, as Rowe and Armitage (1987) acknowledge that
415 "[their method] may be quite conservative for artificially roughened sockets". The
416 methods of O'Neill and Reese (1999), Canadian Foundation Engineering Manual
417 (2006) and AASHTO (2008) also provide similar results to the DEM^{3D} models with
418 $RF < 0.050$, while they are again conservative for higher RF values (see **Fig. 12**).
419 Again, this can be explained by the fact that these formulations are based on the
420 recommendations by Horvath and Kenny (1979) and Rowe and Armitage (1987).
421 Finally, DEM^{3D} results in this study provide $f_{ave,0.01D}$ estimates that are significantly
422 lower than those provided by the formulation by Seidel and Collingwood (2001). The
423 reasons for this discrepancy, or why Seidel and Collingwood (2001) predict
424 significantly higher $f_{ave,0.01D}$ values than other authors, are not clear.

425 Finally, **Fig. 13** compares, for sockets constructed in sandstone (S2, S3) and gneiss,
426 the (i) $\alpha = f_{ave,0.01D}/\sigma_c$ values obtained using the DEM^{3D} model, with (ii) load test
427 data and curves proposed by Pells et al. (1980) (see **Fig. 13**(a)), by Williams and
428 Pells (1981) (see **Fig. 13**(b)), and by Seidel and Collingwood (2001), after they

considered the load tests compiled by Kulhawy and Phoon (1993) (see **Fig. 13**(c)). (Note that these α values correspond to a special case of Eq. (3) when $\beta = 1$; however, α is used, since α is the usual symbol to relate socket side shear resistance and UCS). It can be noted that the DEM^{3D} numerical results: (i) are in a good agreement with α values reported by Pells et al. (1980) (note, however, that their design curves do not capture the variability measured in the load tests), (ii) reproduce well the range of responses measured in real pile reported in curves and data proposed by Williams and Pells (1981) even for several rocks with different strengths within the medium strength range, and (iii) are again consistent with the data compiled by Kulhawy and Phoon (1993) for sockets with different roughness constructed in medium strength rock, and with the design curves proposed by Seidel and Collingwood (2001) to consider the influence of socket roughness.

In any case, and although the discussion above is somewhat speculative due to the ever-existing difficulties to reproduce the real field behavior, and to interpret field tests conducted by others, it strongly suggests that, when properly calibrated, the DEM^{3D} models employed herein can be an adequate tool to estimate the influence of the socket roughness on the average shaft resistance of real piles.

4 Conclusions

The side shear resistance of rock-sockets heavily depends on the roughness of the socket interface. Many empirical criteria developed to assess the side shear resistance of rock sockets, however, do not consider the influence of roughness, providing estimates that only depend on the uniaxial compressive strength (UCS) of the weaker material at the rock-concrete interface. Although there are also empirical

452 criteria that consider the socket roughness, they often provide widely variable
453 estimations of side shear resistance, especially for sockets with higher roughness.

454 This paper shows that discrete numerical models constructed with DEM^{3D} can be
455 employed to (i) reproduce the load-settlement behavior of rock sockets with different
456 roughness and (ii) to estimate their side shear resistance. In particular, results show
457 that DEM^{3D} is able to reproduce the range of load test results measured in practice
458 (or obtained analytically, when analytical solutions are available) for sockets with
459 similar roughness values, and constructed in rocks with UCS values in the medium
460 strength range of, approximately, 10–100 MPa. Results of this research also suggest
461 that sockets drilled with standard tools in soft to medium rock tend to be relatively
462 smooth, unless they are artificially roughened with special tools, and that the
463 commonly employed settlement threshold of 1% of socket diameter could represent
464 the settlement value beyond which significant degradation of asperities at the rock-
465 concrete interface begins to occur, especially for sockets with greater roughness.

466 The main advantage of the numerical pile load-tests employed herein is that they
467 are cheaper and faster than field tests, as they are relatively easy to calibrate, using
468 only laboratory tests results from (i) uniaxial compression strength tests and (ii) direct
469 shear tests under constant normal stiffness boundary conditions. They also allow a
470 more detailed quantification of the influence of roughness than many empirical
471 methods developed using field test data.

5 Data Availability Statement

Some or all data, models, or code that support the findings of this study are available from the corresponding author upon reasonable request (scanned test data; analysis results).

6 Acknowledgement

The first author has received during 2018 the scholarship for PhD research provided by the José Entrecanales Ibarra Foundation. This support is gratefully acknowledged. Also, the authors would like to thank Dr. C. Haberfield, Dr. J. P. Seidel, and Dr. B. Collingwood, for kindly providing data.

7 References

AASHTO (American Association of State Highway and Transportation Officials). (2008). “LRFD bridge design specifications.” Washington, DC.

Arioglu, E., Seker, P. T., and Gokce, H. B. (2018). “Discussion on empirical methods for determining shaft bearing capacity of semi-deep foundations socketed in rocks.” *J. Rock Mech. Geotech. Eng.,* 10(3), 603–606. https://doi.org/10.1016/j.jrmge.2018.01.003.

Bahaaddini, M., Sharrock, G., and Hebblewhite, B. K. (2013). “Numerical direct shear tests to model the shear behaviour of rock joints.” *Comput. Geotech.,* 51: 101–115. https://doi.org/10.1016/j.compgeo.2013.02.003.

Barton, N.R., Choubey, V. (1977). “The shear strength of rock joints in theory and practice”. *Rock Mech. Rock. Eng.,* 10: 1–54. https://doi.org/10.1007/BF01261801.

Barton, N.R., Bandis, S., Bakhtar, K. (1985). “Strength, deformation and conductivity coupling of rock joints”. *Int. J. Rock Mech. Min. Sci. Geomech. Abstr.,* 22(3), 121–140. https://doi.org/10.1016/0148-9062(85)93227-9.

Basarkar, S. S., and Dewaikar, D. M. (2006). “Load transfer characteristics of socketed piles in Mumbai region.” *Soils Found.,* 46(2), 247–257. https://doi.org/10.3208/sandf.46.247.

500 Baycan, S. (1996). “Field performance of expansive anchors and piles in rock.” Ph.D.
501 thesis. Department of Civil Engineering, Monash University, Melbourne,
502 Australia.

503 Canadian Geotechnical Society. (2006). *Canadian Foundation Engineering Manual.*
504 4th edition. Canadian Geotechnical Society. Calgary, Canada.

505 Carrubba, P. (1997). “Skin friction of large-diameter piles socketed into rock.” *Can.*
506 *Geotech. J.,* 34(2), 230–240. https://doi.org/10.1139/t96-104.

507 Collingwood, B. (2000). “The effects of construction practices on the performance of
508 rock socketed bored piles.” Ph.D. thesis, Department of Civil Engineering,
509 Monash University, Melbourne, Australia.

510 Dai, G., Salgado, R., Gong, W., and Zhu, M. (2017). “The effect of sidewall
511 roughness on the shaft resistance of rock-socketed piles.” *Acta Geotechnica,*
512 12(2), 429–440. https://doi.org/10.1007/s11440-016-0470-8.

513 Ding, X., Zhang, L., Zhu, H., and Zhang, Q. (2014). “Effect of Model Scale and
514 Particle Size Distribution on PFC3D Simulation Results.” *Rock Mech. Rock*
515 *Eng.,* 47(6), 2139-2156. https://doi.org/10.1007/s00603-013-0533-1.

516 Gloss, G. H., and Briggs, O. H. (1983). “Rock sockets in soft rock.” *J. Geotech. Eng.,*
517 109(4): 525–535. https://doi.org/10.1061/(ASCE)0733-9410(1983)109:4(525).

518 Gu, X. F., Seidel, J. P., and Haberfield, C. M. (2003). “Direct shear test of sandstone-
519 concrete joints.” *Int. J. Geomech.,* 3, 21–33.
520 https://doi.org/10.1061/(ASCE)1532-3641(2003)3:1(21).

521 Gupton, C., and Logan, T. (1984). “Design guidelines for drilled shafts in weak rocks
522 of South Florida.” *Proc., South Florida Annual ASCE Meeting*, ASCE, Miami,
523 Florida.

524 Gutiérrez, M. (2013). “Shear resistance for concrete dams: Laboratory tests.” Master
525 Thesis. Department of Hydraulic and Environmental Engineering, Norwegian
526 University of Science and Technology. Trondheim.

527 Gutiérrez-Ch, J. G., Senent, S., Melentijevic, S., and Jimenez, R. (2018). “Distinct
528 element method simulations of rock-concrete interfaces under different
529 boundary conditions.” *Eng. Geol.,* 240, 123–139.
530 https://doi.org/10.1016/j.enggeo.2018.04.017.

531 Haberfield, C. M. (2013). “Performance of footings in rock based on serviceability.”
532 *Australi. Geomech. J.,* 48(1), 1–49.

533 Hassan K. M., O’Neill, M. W., Sheikh, S. A., and Ealy, C.D. (1997) “Design method
534 for drilled shafts in soft argillaceous rock.” *J. Geotech. Geoenviron. Eng.,* 123(3),
535 272-280. https://doi.org/10.1061/(ASCE)1090-0241(1997)123:3(272).

536 Hooley, P., and Lefroy, S. R. (1993). “The ultimate frictional resistance mobilized by
537 bored piles in over-consolidated clays and socketed into weak and weathered
538 rock.” *The Engineering Geology of Weak Rock*. Rotterdam: Balkema, 447-55

539 Horvath, R. G., and Kenney, T. C. (1979). “Shaft resistance of rock-socketed drilled
540 piers.” *Proc., Symp., on Deep Found.,* ASCE, 182-214. Atlanta, USA.

541 Horvath, R. G., Kenney, T. C., and Kozicki, P. (1983). “Methods for improving the
542 performance of drilled piers in weak rock.” *Can. Geotech. J.,* 20(4), 758–772.
543 https://doi.org/10.1139/t83-081.

544 Itasca Consulting Group Inc. (2014). PFC Manual, Version 5.0. (Minneapolis,
545 Minnesota).

546 Ivars, D. M., Potyondy, D. O., Pierce, M., and Cundall, P. A. (2008). “The smooth-
547 joint contact model.” *Proc., 8th. World Congress on Computational Mech. - 5th.*
548 *European Congress on Computational Methods in Applied Sci. and Eng.*
549 Venice, Italy.

550 Ivars, D. M., Pierce, M. E., Darcel, C., Reyes-Montes, J., Potyondy, D. O., Young,
551 R. P., and Cundall, P. A. (2011). “The synthetic rock mass approach for jointed
552 rock mass modelling.” *Int. J. Rock Mech. Min. Sci.,* 48, 219–244.
553 http://dx.doi.org/10.1016/j.ijrmms.2010.11.014.

554 Jeong, S., Ahn, S., and Seol, H. (2010). “Shear load transfer characteristics of drilled
555 shafts socketed in rocks.” *Rock Mech. Rock Eng.,* 43(1), 41–54.
556 https://doi.org/10.1007/s00603-009-0026-4.

557 Kaderabek. T. J., and Reynolds, R. T. (1981). “Miami limestone foundation design
558 and construction.” *J. Geotech. Eng.,* 107(7), 859–872.

559 Kishida, H., Uesugi, M. (1987). “Tests of the interface between sand and steel in the
560 simple shear apparatus”. *Géotechnique*, 37(1), 45–52.
561 https://doi.org/10.1680/geot.1987.37.1.45.

562 Kodikara, J.K., Johnston, I.W. (1994). “Shear behaviour of irregular triangular rock-
563 concrete joints”. *Int. J. Rock Mech. Min. Sci. Geomech. Abstr.,* 31, 313–322.
564 https://doi.org/10.1016/0148-9062(94)90900-8.

565 Kulhawy, F. H., and Phoon, K. K. (1993). “Drilled shaft resistance in clay soil to rock.”
566 *Proc., Conference on Design and Performance of Deep Foundations: Piles and*
567 *Piers in Soil and Soft Rock., ASCE. Geotech. Spec. Publ.,* 38, 172–183. New
568 York, USA.

569 Kulkarni, R. U., and Dewaikar D. M. (2016). “An empirical approach to assess socket
570 friction and point resistance of axially loaded rock socketed piles of Mumbai
571 region.” *Int. J. Geotech. Eng.,* 11(5), 479–486.
572 https://doi.org/10.1080/19386362.2016.1237607.

573 Matich, M. A. J., and Kozicki, P. (1967). “Some load tests on drilled cast in place
574 concrete caissons.” *Can. Geotech. J.,* 4(4): 367–375.
575 https://doi.org/10.1139/t67-065.

576 Meigh, A. C., and Wolshi, W. (1979). “Design parameters for weak rocks.” *Proc., 7th*
577 *European Conf. on Soil Mech. Found. Eng.,* 55–57. Brighton, British
578 Geotechnical Society.

579 Melentijevic, S., and Olalla, C. (2014). “Different FEM models for simulation of the
580 Osterberg load test in rock shafts.” *ISRM Regional Symp. EUROCK 2014*.
581 London, United Kingdom.

582 Nam, M. S., and Vipulanandan, C. (2008). “Roughness and unit side resistances of
583 drilled shafts socketed in clay shale and limestone.” *J. Geotech. Geoenviron.*
584 *Eng.,* 134(9), 1272–1279. https://doi.org/10.1061/(ASCE)1090-
585 0241(2008)134:9(1272).

586 Ng, C. W. W., Yau, T. L. Y., Li, J. H. M., and Tang, W. H. (2001). ‘‘Side resistance
587 of large diameter bored piles socketed into decomposed rocks.’’ *J. Geotech.*
588 *Geoenviron. Eng.,* 127(8), 658–669. https://doi.org/10.1061/(ASCE)1090-
589 0241(2001)127:8(642).

590 O’Neill, M. W., Townsend, F. C., Hassan, K. M., Buller, A., and Chan, P. S. (1996).
591 “Load transfer for drilled shafts in intermediate geomaterials.” U.S. Department
592 of Transportation, FHWA-RD- 95–172, Final Report.

593 O’Neill, M. W., and Reese, L. C. (1999). “Drilled shafts: construction procedures and
594 design methods.” FHWA-IF-99-025, Federal Highway Administration, U.S.
595 Department of Transportation, Washington, DC.

596 Patton, F.D. (1966). Multiple modes of shear failure in rock. 1st ISRM Congress.
597 Lisbon, Portugal, 509–513.

598 Pells, P. J. N., Rowe, R. K., and Turner, R. M. (1980). “Experimental investigation
599 into shear for socketed piles in sandstone.” *Proc., Int. Conf. on Struct. Found.*
600 *on Rock,* 1, 291–302. Sydney, Australia. Publ Rotterdam: A A Balkema.
601 https://doi.org/10.1016/0148-9062(81)90887-1.

602 Pells, P. J. N., Mostyn, G., and Walker, B. F. (1998). “Foundations on sandstone and
603 shale in the Sydney region.” *Australi. Geomech.* 33(3), 17–29.

604 Potyondy, D. O. (2012). “A flat-jointed bonded-particle material for hard rock.” *46th*
605 *US Rock Mechanics/Geomechanics Symposium*. Chicago, Illinois.

606 Potyondy, D. O. (2015). “The bonded-particle model as a tool for rock mechanics
607 research and application: current trends and future directions.” *Geosyst. Eng.,*
608 18, 1–28. http://dx.doi.org/10.1080/12269328.2014.998346.

609 Ragan, D.M. (2009). “Structural geology: an introduction to geometrical techniques.”
610 Cambridge (UK): Cambridge University Press.
611 https://doi.org/10.1017/CBO9780511816109.

612 Rezazadeh, S., and Eslami, A. (2017). “Empirical methods for determining shaft
613 bearing capacity of semi-deep foundations socketed in rocks.” *Int. J. Rock Mech.*
614 *Geotech. Eng.,* 9(6), 1140–1151. https://doi.org/10.1016/j.jrmge.2017.06.003.

615 Rosenberg, P., and Journeaux, N. L. (1976). “Friction and end bearing tests on
616 bedrock for high capacity socket design.” *Can. Geotech. J.,* 13(3), 324–333.
617 https://doi.org/10.1139/t76-033.

618 Rowe, R. K., and Armitage, H. H. (1987). “A design method for drilled piers in soft
619 rock.” *Can. Geotech. J.,* 24(1), 126–142. https://doi.org/10.1139/t87-011.

620 Sagong, M., Paik, K., and Kim, D. (2007). “A new approach to estimate side
621 resistance of rock socketed drilled shafts.” *Soils Found.,* 47(2), 415–421.
622 https://doi.org/10.3208/sandf.47.415.

623 Seidel, J. P., and Haberfield, C. M. (1995). “The axial capacity of pile sockets in rocks
624 and hard soils.” *Ground Eng.,* 28(2), 33–38.

625 Seidel, J. P., and Collingwood, B. (2001). “A new socket roughness factor for
626 prediction of rock socket shaft resistance.” *Can. Geotech. J., 38(1)*, 138–153.
627 https://doi.org/10.1139/t00-083.

628 Seo, H., Prezzi, M., and Salgado, R. (2013). “Instrumented static load test on rock-
629 socketed micropile.” *J. Geotech. Geoenviron. Eng.,* 139(12), 2037-2047.
630 https://doi.org/10.1061/(ASCE)GT.1943-5606.0000946.

631 Seol, H. I., and Jeong, S. S. (2007). “Shaft resistance characteristics of rock-
632 socketed drilled shafts based on pile load tests.” *J. Korean Geotech. Soc.,* 23(9),
633 51–63

634 Seol, H.I., Jeong, S. S., and Cho, S. (2009). “Analytical method for load-transfer
635 characteristics of rock-socketed drilled shafts.” *J. Geotech. Geoenviron. Eng.,*
636 135(6), 778-789. https://doi.org/10.1061/(ASCE)1090-0241(2009)135:6(778).

637 Serrano, A., Olalla, C., and Aguilar, D. (2008). “Resistencia por fuste de pilotes
638 empotrados en roca: Estudio comparativo entre distintos métodos de cálculo y
639 normativas.” *Ingeniería Civil* 149, 1–14. (in Spanish).

640 Serrano, A., Olalla, C., and Galindo, R. A. (2015). “Shaft resistance of a pile in rock
641 based on the modified Hoek–Brown criterion.” *Int. J. Rock Mech. Min. Sci.,* 76,
642 138–145. https://doi.org/10.1016/j.ijrmms.2015.03.007.

643 Technical Building Code CTE, 2006. Basic document. Energy saving, CTE-DB-HE.
644 Spanish Ministry of Housing. Madrid, Spain. http://www.codigotecnico.org.

Toh, C. T., Ooi, T. A., Chiu, H. K., Chee, S. K., and Ting, W. H. (1989). “Design parameters for bored piles in a weathered sedimentary formation.” *Proc., 12th Int. Conf. on Soil Mech. Found. Eng*., 2,1073–1078. Rio de Janeiro.

Walter, D. J., Burwash, W. J., and Montgomery, R. A. (1997). “Design of large-diameter drilled shafts for Northumberland Strait bridge project.” *Can. Geotech. J.,* 34(4). 580–587. https://doi.org/10.1139/t97-036.

Wang, J., Dove, J. E., Gutierrez, M. S. (2007). Anisotropy-based failure criterion for interphase systems. *J. Geotech. Geoenviron. Eng.,* 133(5), 599–608. https://doi.org/10.1061/(ASCE)1090-0241(2007)133:5(599).

Whitaker, T., Cooke, R. W. (1966). “An investigation of the shaft and base resistances of large bored piles in London Clay”. *Proc., Symp., of Large Bored Piles,* 7-49. London, UK.

Williams, A. F. (1980). “The side resistance of piles socketed into weak rock.” Ph.D. Thesis. Department of Civil Engineering, Monash University, Melbourne, Australia.

Williams, A. F., Johnston, I. W., and Donald, I. B. (1980). “The design of socketed piles in weak rock.” *Proc., Int. Conf. Struct. Found. Rock,* 1, 327–347. Sydney, Australia.

Williams, A. F., and Pells, P. J. N., 1981. “Side resistance in sandstone, mudstone, and shale.” *Can. Geotech. J.,* 18(4), 502–513. https://doi.org/10.1139/t81-061.

Zhang, L., and Einstein, H. H. (1998). “End bearing capacity of drilled shafts in rock.” *J. Geotech. Geoenviron. Eng.,* 124(7), 574–584. https://doi.org/10.1061/(ASCE)1090-0241(1998)124:7(574).

Zhang, L. (2004). “Drilled shafts in rock: analysis and design.” London (UK): Balkema.

Table 1. Micro-mechanical properties fitted from the UCS tests employed in the calibration of intact material models

Type	Property	(I)	(II)	(III)	(IV)	(V)
Particle micromechanical properties	E^*(GPa)	1.70	1.90	27.00	43.00	26.20
	$k^* = k_n/k_s$	1.35	1.45	2.75	3.25	3.00
	Friction angle ∅ (º)	32	35	30	35	30
	Ball density, $\rho(kg/m^3)$	2500	2550	2500	2690	2500
	Minimum radius, R_{min} (mm)	1.0	1.0	0.8	0.8	1.0
	R_{max}/R_{min}	1.4	1.4	1.5	1.5	1.4
Flat-joint micromechanical properties	$\overline{E^*}$(GPa)	1.70	1.90	27.00	43.00	26.20
	$\overline{k^*}$	1.35	1.45	2.75	3.25	3.00
	c (MPa)	4.85	7.90	13.55	40.80	18.80
	σ_t (MPa)	2.8	3.5	6.0	20.0	9.0
	FJ bonding ratio, c/σ_t	1.73	2.26	2.26	2.04	2.08
	Bonded fraction, ϕ_B	0.88	0.90	0.93	0.96	0.94
	Gapped fraction, ϕ_G	0.12	0.10	0.07	0.04	0.06
	Initial gap, g_o (mm)	0.05	0.05	0.05	0.05	0.05

(I) Sandstone-S2, (II) sandstone-S3, (III) concrete-C1; (IV) gneiss, (V) concrete-C2

Table 2. Macro-mechanical properties for the UCS tests employed in the calibration of intact material models

Sample	Macro-properties	Experimental	PFC^{2D}
		Ave.	Ave.
Gneiss^{+}	σ_c (MPa) ± SD	158.87 ± 7.11 $(n = 3)$	158.84 ± 7.14 $(n = 10)$
	E (GPa) ± SD	50^{*}	50.23 ± 0.40 $(n = 10)$
	ν ± SD	0.25^{*}	0.24 ± 0.03 $(n = 10)$
Concrete-C2^{+}	σ_c (MPa) ± SD	62.20 ± 0.74 $(n = 4)$	62.12 ± 3.01 $(n = 10)$
	E (GPa) ± SD	30^{*}	29.98 ± 0.26 $(n = 10)$
	ν ± SD	0.20^{*}	0.20 ± 0.02 $(n = 10)$
Sandstone-S2^{++}	σ_c (MPa) ± SD	11.49 ± 3.19 $(n = 8)$	11.59 ± 0.97 $(n = 10)$
	E (GPa) ± SD	1.98 ± 0.68 $(n = 5)$	2.01 ± 0.02 $(n = 10)$
	ν ± SD	0.10 ± 0.00 $(n = 3)$	0.10 ± 0.01 $(n = 10)$
Sandstone-S3^{++}	σ_c (MPa) ± SD	21.77 ± 1.19 $(n = 8)$	21.65 ± 1.43 $(n = 10)$
	E (GPa) ± SD	3.25 ± 0.39 $(n = 5)$	2.32 ± 0.02 $(n = 10)$
	ν ± SD	0.10 ± 0.00 $(n = 3)$	0.11 ± 0.01 $(n = 10)$
Concrete-C1^{++}	σ_c (MPa) ± SD	40 ± 0.33 $(n = 3)$	39.87 ± 2.73 $(n = 10)$
	E (GPa) ± SD	29.95 ± 0.08 $(n = 3)$	30.08 ± 0.23 $(n = 10)$
	ν ± SD	0.20^{*}	0.20 ± 0.02 $(n = 10)$

SD = Standard Deviation, n = number of tests, *SD not reported in the original reference
$^{+}$ Experimental from Gu et al. (2003), $^{++}$ Experimental from Gutiérrez (2013)

Table 3. Fitted parameters (with DEM^{2D} models) of SJCM on planar interface employed for validation

SJCM parameters (PFC^{2D})	Sandstone(S2)-concrete(C1)	Sandstone(S3)-concrete(C1)	Gneiss-concrete(C2)
Joint normal stiffness, $k_{n\,SJ}$ (MPa/mm)	10	10	10
Joint shear stiffness, $k_{s\,SJ}$ (MPa/mm)	5	2	2
Joint coefficient of friction, μ_{SJ} ($\tan\emptyset$ (º))	0.70	0.70	0.60

Table 4. Comparison of joint macroscopic parameters for direct shear tests with DEM^{2D} results and measured in the laboratory by Gu et al. (2003) and Gutiérrez (2013)

Joint macroscopic parameters	Experimental from Gu et al. (2003)	Numerical (PFC^{2D})	Experimental from Gu et al. (2003)	Numerical (PFC^{2D})	Experimental from Gutiérrez (2013)	Numerical (PFC^{2D})
System normal stiffness, K_n, (MPa/mm)	-	9.50	-	10.30	-	16.49
System shear stiffness, K_s, (MPa/mm)	1.84	1.81	1.37	1.36	2.51	2.53
Friction angle, $\tan \emptyset$ (º)	35.37	34.99	34.96	34.99	31.22	31.10

Table 5. Particle size distributions in the numerical models of rock-socketed piles testing

Material	Zone	Minimum radius, R_{min} (cm)	R_{max}/R_{min}
Rock (Sandstone(S2,S3) and gneiss)	Zone 1	1.00	1.5
	Zone 2	1.50	1.5
	Zone 3	2.25	1.5
Pile (Concrete(C1,C2))	Zone 1	1.00	1.5

Table 6. Axial load supported by rock-socketed piles with different roughness for socket head settlement of 2 % of pile diameter

Tests	Model	Roughness classification*	Roughness Factor, RF	Axial Load, P (kN)
Numerical PFC^{3D} on sandstone-S3	1	R1	0.000	20.2
	2	R2	0.010	148.7
	3	R3	0.025	451.7
	4	R4	0.050	941.1
	5	R4	0.085	1675.4
	6	R4	0.106	2438.9
Field tests on shale by Horvath et al. (1983)	P1	R4	0.036	3996.5
	P2	R4	0.076	5189.3
	P3	R4	0.100	7273.9

* Roughness classification proposed by Pells et al. (1980), see **Table 9**

Table 7. Socket roughness resulting by different drilling method on rock-socketed piles

Drilling tool	Average height of asperities, h_m, (mm)	Type of rock	σ_c (MPa)	Reference of load test data
Auger[b]	75[c]	Shale	0.48	Matich and Kozicki 1967
Diamond tube	< 4[e]	Sandstone	14	Pells et al. 1980
Diamond tube	< 1[e]	Sandstone	6	Pells et al. 1980
Rock roller	< 4[e]	Sandstone	6	Pells et al. 1980
Rock roller	< 1[e]	Sandstone	30	Pells et al. 1980
Auger	< 10[e]	Sandstone	6	Pells et al. 1980
Three flight auger	5.7[d]	Mudstone	0.83	Williams 1980
Three flight auger[b]	12.2[d]	Mudstone	0.55	Williams 1980
Three flight auger[b]	4.8[d]	Mudstone	0.59	Williams 1980
Core barrel[b]	10[d]	Mudstone	0.58	Williams 1980
Bucket auger	7.3[d]	Mudstone	2.46	Williams 1980
Bucket auger[b]	17.3[d]	Mudstone	2.30	Williams 1980
Bucket auger	5.9[d]	Mudstone	2.30	Williams 1980
Bucket auger	5.2[d]	Mudstone	3.06	Williams 1980
Auger	12.7[c]	Shale	5.4, 5.6, 11.1	Horvath et al. 1983
Auger + Special pneumatic tool[b]	24.1[c]	Shale	5.5	Horvath et al. 1983
Auger + Special pneumatic tool[a]	24.1[c]	Shale	10.4	Horvath et al. 1983
Auger reaming tool[a]	31.5[c]	Shale	6.75	Horvath et al. 1983
Auger[b]	76[c]	Sandstone	8.36 – 9.26	Gloss and Briggs 1983
Auger	< 12.5[c]	Clay shale	0.5 - 5	O'Neil et al. 1996
Auger + grooving teeth tool[a]	11.1[d]	Siltstone	3.3 – 7.2	Baycan 1996
Auger + grooving teeth tool[a]	8.2[d]	Siltstone	3.3 – 7.2	Baycan 1996
Downhole jacket + pneumatic grooving tool[a]	100[c]	Mudstone	3.2	Walter et al. 1997
Downhole jacket + pneumatic grooving tool[a]	100[c]	Siltstone	8.9	Walter et al. 1997
Downhole jacket + pneumatic grooving tool[a]	100[c]	Sandstone	11.6	Walter et al. 1997
Auger	10.2[d]	Sandstone	-	Collingwood (2000)
Flight auger + circumferential groves cut (WRT1)[a]	7.1[d]	Shale	7.5 – 20	Collingwood (2000)
Flight auger + circumferential groves cut (WRT1)[a]	9[d]	Shale	1.5 – 7.5	Collingwood (2000)
Flight auger + circumferential groves cut (WRT1)[a]	16.1[d]	Siltstone	0.8 – 1.35	Collingwood (2000)
Auger	6[d]	Sandstone	6	Collingwood (2000)
Auger	7[d]	Conglomerate	6	Collingwood (2000)
Core barrel	2.8[d]	Basalt	50 – 75	Collingwood (2000)
Core barrel	4.1[d]	Basalt	75 – 100	Collingwood (2000)
Auger	2.5[c]	Clay shale	1.2	Nam and Vipulanandan 2008
Core barrel	3.7[c]	Clay shale	1.2	Nam and Vipulanandan 2008
Auger	1.6 – 2.6[c]	Clay shale	6	Nam and Vipulanandan 2008
Core barrel	4.2[c]	Clay shale	2.1	Nam and Vipulanandan 2008
Auger	2.2[c]	Limestone	10	Nam and Vipulanandan 2008
Core barrel	3.5[c]	Limestone	10	Nam and Vipulanandan 2008
RCD	1 – 5.1[c]	Granite	100 – 150	Jeong et al. 2010
RCD	1 – 4[c]	Gneiss	30 – 130	Jeong et al. 2010
Bit	1 – 7[c]	Gneiss	5 – 50	Jeong et al. 2010

[a] Artificial roughening practices
[b] Then roughened (the tool used to increase the roughness is not indicated)
[c] Provided in reference of load test data
[d] Estimated by the authors using roughness profiles provided in reference of load test data
[e] Estimated using roughness classification proposed by Pells et al. (1980), see **Table 9**

Table 8. Empirical factors α and β for average side shear resistance design assuming a relationship of type $f_{ave}[\text{MPa}] = \alpha(\sigma_c[\text{MPa}])^{\beta}$

Design method	α	β
Rosenberg and Journeaux (1976)	1.11	0.51
Horvath and Kenney (1979)		
- For large piles – diameter ≥ 410 mm		
a) Lower bound	0.20	0.50
b) Upper bound	0.25	0.50
- For small piles – diameter < 410 mm		
a) Lower bound	0.25	0.50
b) Upper bound	0.33	0.50
Meigh and Wolski (1979)	0.22	0.60
Kaderbeck and Reynolds (1981)	0.30	1.00
Williams et al. (1980)	0.44	0.36
Australian Piling Code (1980)	0.15	1.00
Horvath et al. (1983)		
a) Smooth socket (conservative lower value)	0.20	0.50
b) Rough socket (conservative lower value)	0.30	0.50
c) Considering roughness factor, RF	$0.80RF$	0.45
Gupton and Logan (1984)	0.20	1.00
Rowe and Armitage (1987)		
a) For R1, R2, R3[b], $b = 0.45$	$0.70b$	0.50
b) For R4[b], $b = 0.60$	$0.70b$	0.50
Toh et al. (1989)	0.25	1.00
Hooley and Lefroy (1993)		
a) For $0.25 < \sigma_c$	0.30	1.00
b) For $0.25 \leq \sigma_c \leq 3.00$ MPa	0.15	0.50
c) For $\sigma_c > 3.00$ MPa then $f_{ave,peak} = 0.4$ MPa	-	-
Kulhawy and Phoon (1993)		
a) Upper bound	1.34	0.50
b) Lower bound	0.22	0.50
Carrubba (1997)		
a) Lower bound	0.13	0.50
b) Upper bound	0.25	0.50
Zhang and Einstein (1998)		
a) For R1, R2, R3[b]	0.40	0.50
b) For R4[b]	0.80	0.50
O'Neill and Reese (1999)[a], Canadian Foundation Engineering Manual (2006)[a] and American Association of State Highway and Transportation Officials AASHTO (2008)[a]		
a) Smooth socket	0.20	0.50
b) Rough socket	0.30	0.50
c) Very rough socket (i.e., asperities amplitudes more than 10 mm)	0.60	0.50
Technical Building Code, CTE (2006)	0.20	0.50
Basarkar and Dewaikar (2006)[a]	0.40	0.50
Sagong et al. (2007)[a]	0.38	0.51
Rezazadeh and Eslami (2017)[a]	0.36	0.36
Arioglu et al. (2018)[a]	0.36	0.40

Source: Data from O'Neil et al (1996); Serrano et al. (2008).
[a] This correlation has been added by this paper
[b] Roughness classification proposed by Pells et al. (1980), see **Table 9**

Table 9. Roughness classification.

Roughness class	Description
R1	Straight, smooth sided socket, grooves or indentations less than 1-mm deep
R2	Grooves of depth 1-4 mm, width greater than 2-mm, at spacing 50-mm to 200-mm
R3	Grooves of depth 4-10 mm, width greater than 5-mm, at spacing 50-mm to 200-mm
R4	Grooves or undulations of depth > 10-mm, width > 10-mm at spacing 50-mm to 200-mm

Source: Reprinted from *International Journal of Rock Mechanics and Mining Sciences & Geomechanics Abstracts*, Vol. 18(2), P, J. N. Pells, R. K. Rowe, and R. M. Turner, "Experimental investigation into shear for socketed piles in sandstone," pp. 33, © 1981, with permission from Elsevier.

List of Figures

Fig. 1. (a) 3D idealization of a flat joint material (modified from Itasca Consulting Group Inc 2014), (b) notation used to define joint and smooth-joint contacts where θ_p is the joint plan angle, $\hat{n}_j$ is the joint normal unit vector, $\hat{t}_j$ is the joint shear unit vector, and $\hat{n}_c$ and $\hat{t}_c$ are the normal and shear unit vectors, respectively, at each contact point (modified from Ivars et al. 2011).

Fig. 2. (a) sandstone(S2)-concrete(C1) model (grey balls represent concrete particles, yellow balls represent sandstone particles; a total of around 12256 particles), (b) comparison with the direct shear test results conducted on unbonded sandstone(S2)-concrete(C1) planar joint with different normal stresses, σ_n (laboratory data from Gu et al. 2003).

Fig. 3. (a) idealized sub-surface profile and nomenclature where H_s is the height of the overlying soil stratum, H_r is the height of the rock stratum, L is the nominal socket length and R is the socket radius, (b) rock-socketed pile model in DEM^{3D}.

Fig. 4. (a) rock-socketed pile container with zones (as a function of the socket radius, R) corresponding to different particle size distributions, (b) example of an initial particle assembly for a DEM^{3D} numerical test (c) contact-force distribution after isotropic stress installation (black lines represent contact-force intensity and purple spheres represent the “measurement regions”), (d) detection of floating particles (red balls represent floating particles).

Fig. 5. DEM^{3D} model after applying FJCM and SJCM: (a) 3D view and top view of unit normal vectors (purple arrows represent unit normal vector of the SJCM perpendicular to the rock-concrete surface), (b) stereonet projections of unit normal vectors of the SJCM for models with $RF = 0.025$ and $RF = 0.106$ (red points represent the pole vectors of the unit normal vectors). (Note that to facilitate the visualization the particles of body pile are not presented.)

Fig. 6. (a) 3D view of rock-socketed pile for testing in DEM^{3D} where Q_1 and Q_2 are the stresses that represent the self-weight of the upper portion of the pile and the overlying soil stratum, respectively (b) view of the DEM^{3D} models of rock sockets with different roughness RF values.

Fig. 7. Parameters for defining the roughness factor RF (modified from Zhang 2004)

Fig. 8. Comparison of load-settlement responses of rock-socketed piles on sandstone-S3 with different roughness computed with DEM^{3D} models.

Fig. 9. (a) average side shear resistance (f_{ave}) versus socket head settlement (δ) on sandstone-S3, (b) number of cracks versus socket head settlement (δ) on sandstone-S3.

Fig. 10. Average side shear resistance (f_{ave}) versus socket head settlement (δ) on (a) sandstone-S2, (b) gneiss.

Fig. 11. Average side shear resistance (f_{ave}) versus roughness factor (RF) for a pile head movement equivalent to 1% and 2% of the pile diameter on sandstone-S3 computed with DEM^{3D} numerical models.

Fig. 12. Side shear resistance estimation: comparative between DEM^{3D} results (on sandstone-S3) and empirical and analytical criteria.

Fig. 13. DEM^{3D} results compared with design curves proposed (a) by Pells et al. (1980), (b) by Williams and Pells (1981), (c) by Seidel and Collingwood (2001) after incorporated the load tests data of Kulhawy and Phoon (1993).

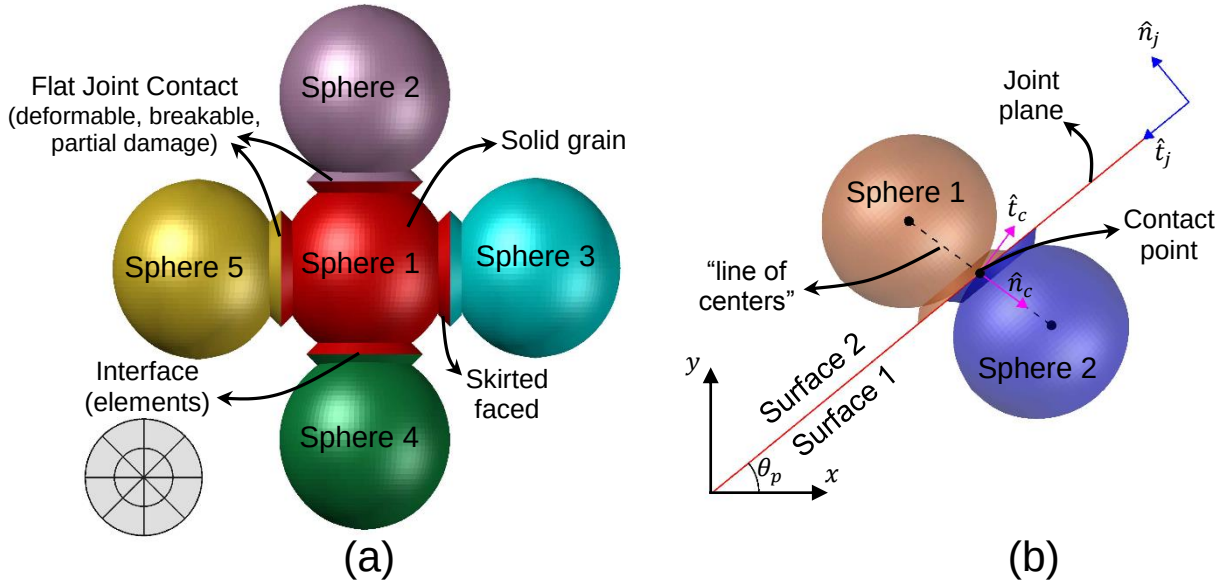

Fig. 1. (a) 3D idealization of a flat joint material (modified from Itasca Consulting Group Inc 2014), (b) notation used to define joint and smooth-joint contacts where θ_p is the joint plan angle, $\hat{n}_j$ is the joint normal unit vector, $\hat{t}_j$ is the joint shear unit vector, and $\hat{n}_c$ and $\hat{t}_c$ are the normal and shear unit vectors, respectively, at each contact point (modified from Ivars et al. 2011).

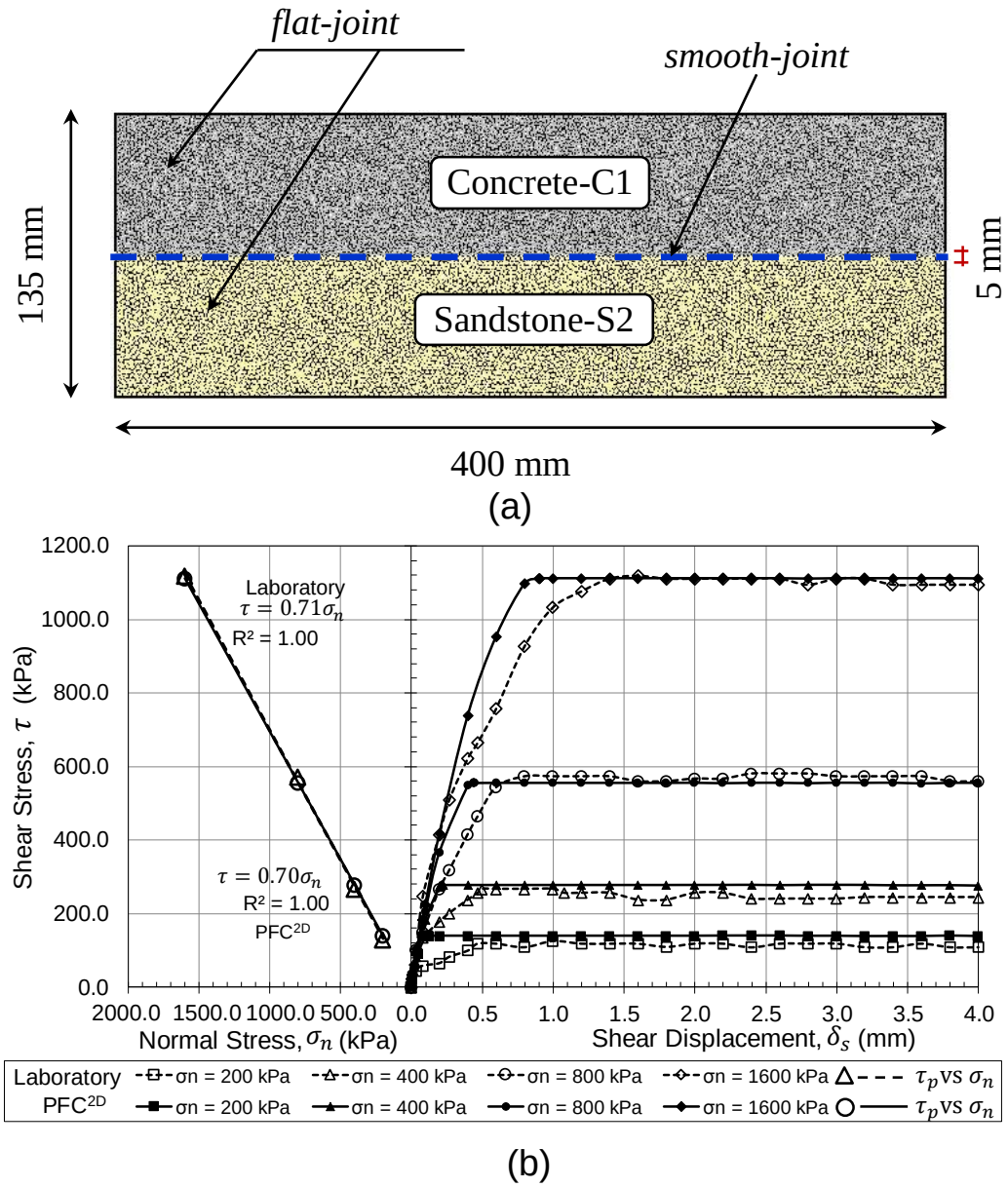

Fig. 2. (a) sandstone(S2)-concrete(C1) model (grey balls represent concrete particles, yellow balls represent sandstone particles; a total of around 12256 particles), (b) comparison with the direct shear test results conducted on unbonded sandstone(S2)-concrete(C1) planar joint with different normal stresses, σ_n (laboratory data from Gu et al. 2003).

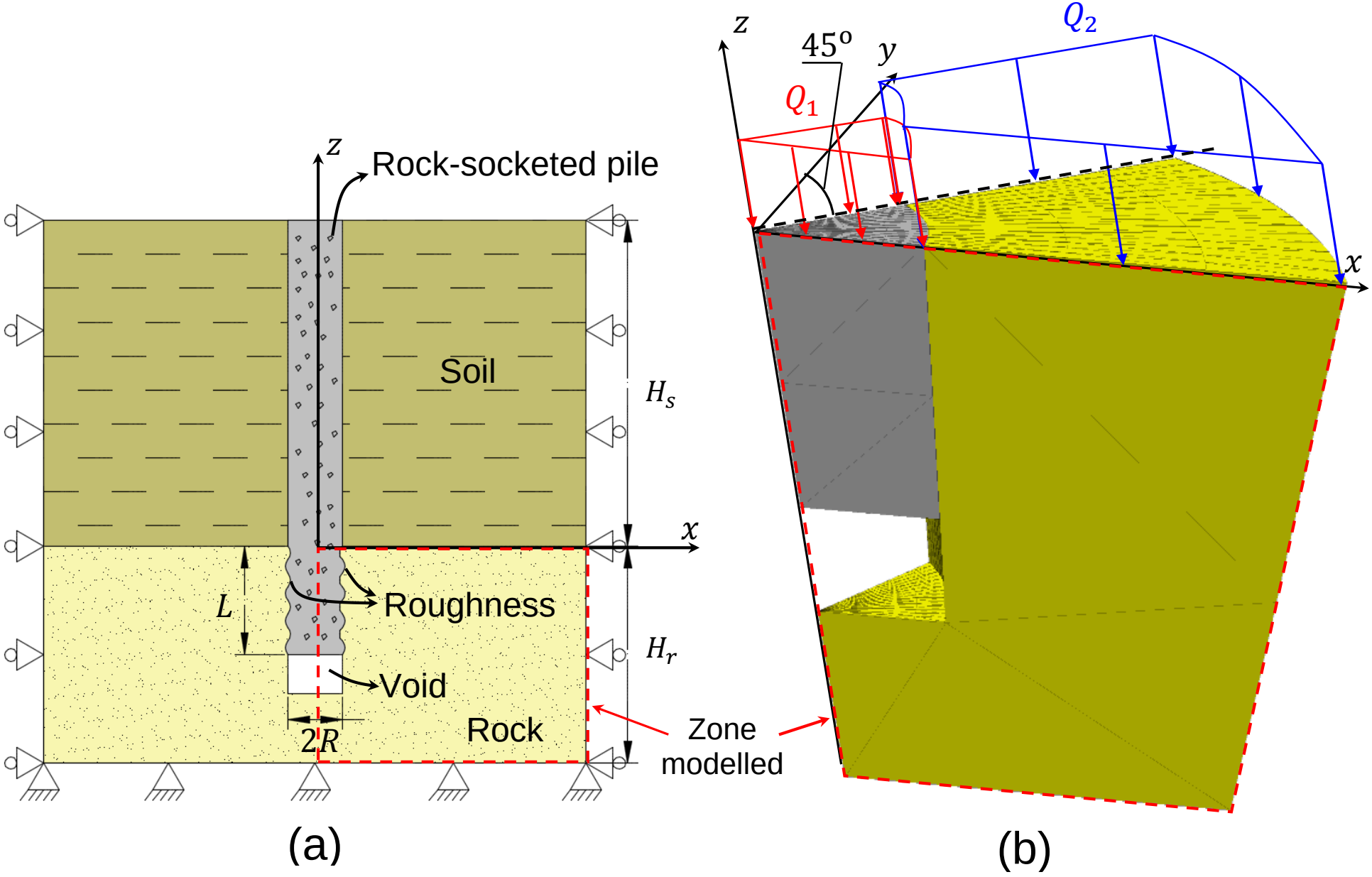

Fig. 3. (a) idealized sub-surface profile and nomenclature where H_s is the height of the overlying soil stratum, H_r is the height of the rock stratum, L is the nominal socket length and R is the socket radius, (b) rock-socketed pile model in DEM^{3D}.

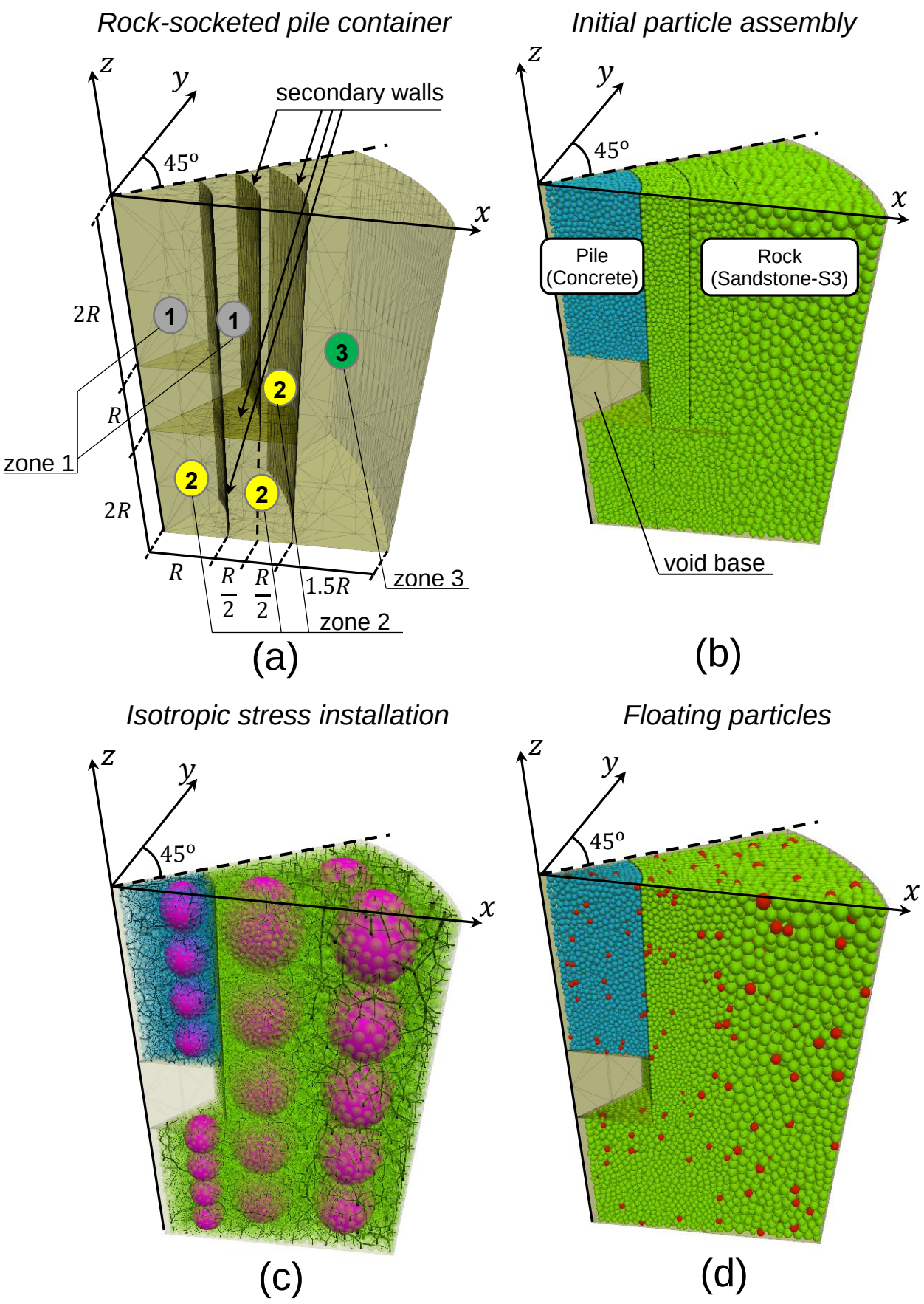

Fig. 4. (a) rock-socketed pile container with zones (as a function of the socket radius, R) corresponding to different particle size distributions, (b) example of an initial particle assembly for a DEM^{3D} numerical test (c) contact-force distribution after isotropic stress installation (black lines represent contact-force intensity and purple spheres represent the "measurement regions"), (d) detection of floating particles (red balls represent floating particles).

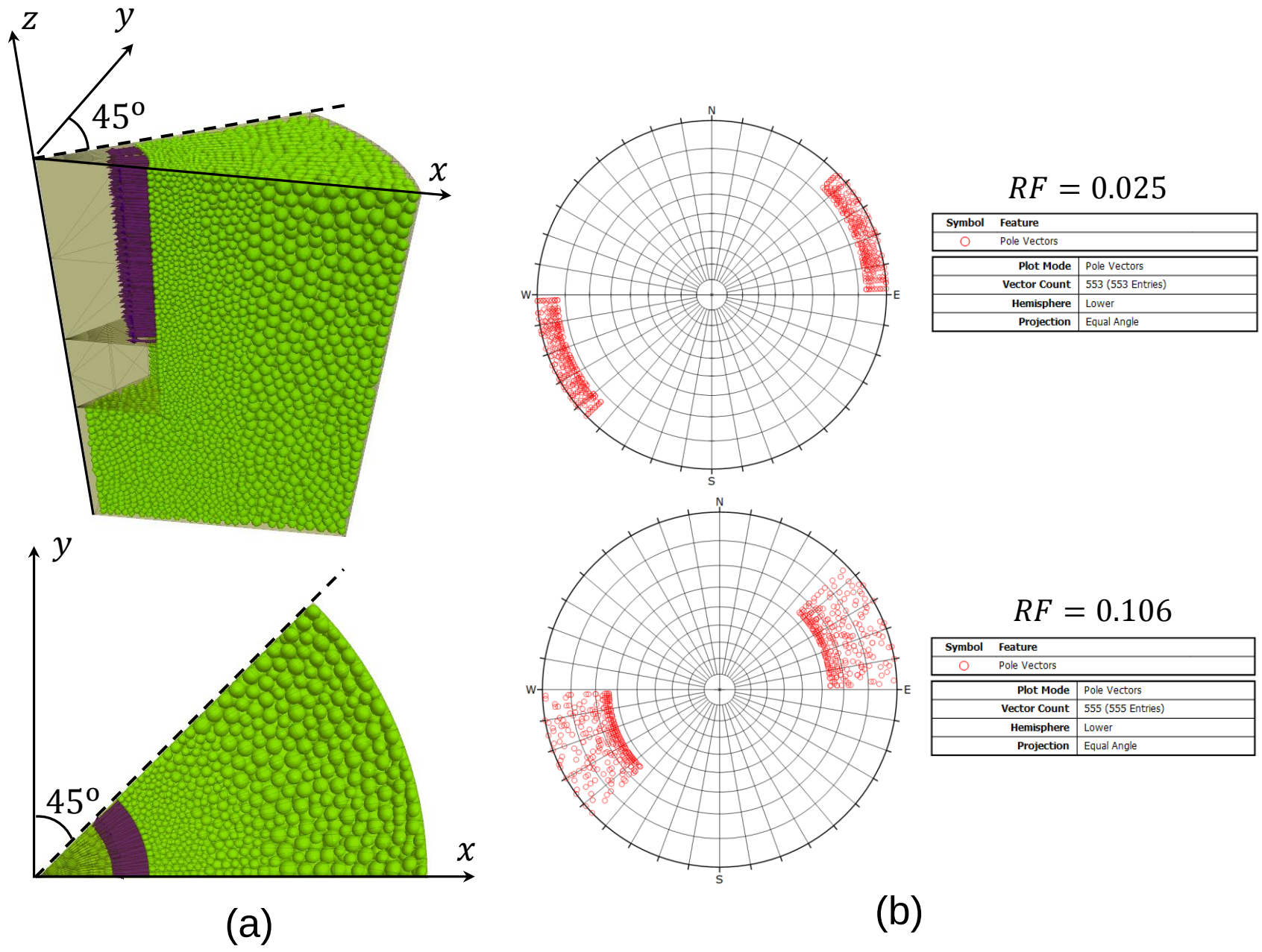

Fig. 5. DEM[3D] model after applying FJCM and SJCM: (a) 3D view and top view of unit normal vectors (purple arrows represent unit normal vector of the SJCM perpendicular to the rock-concrete surface), (b) stereonet projections of unit normal vectors of the SJCM for models with $RF = 0.025$ and $RF = 0.106$ (red points represent the pole vectors of the unit normal vectors). (Note that to facilitate the visualization the particles of body pile are not presented.)

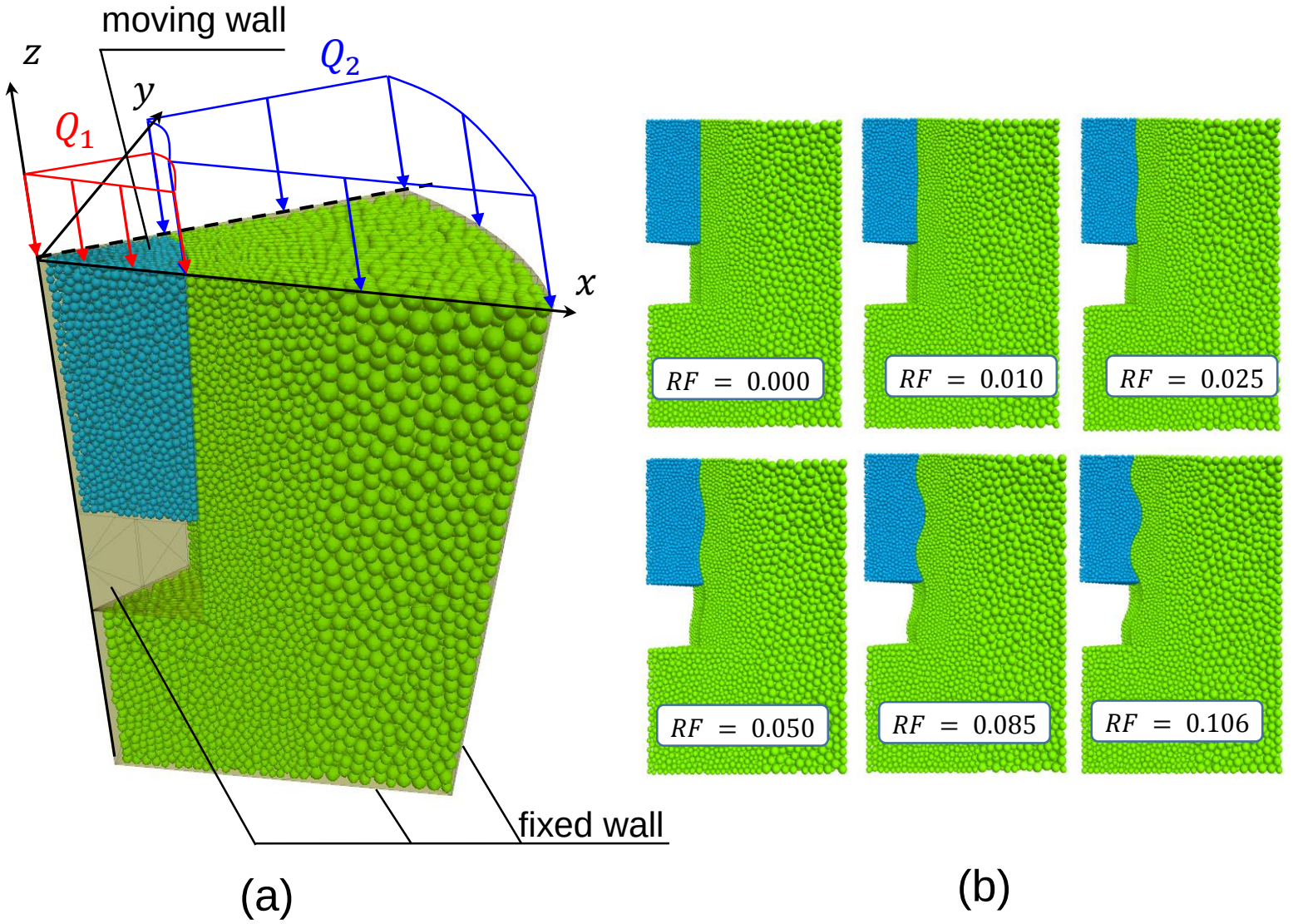

Fig. 6. (a) 3D view of rock-socketed pile for testing in DEM[3D] where Q_1 and Q_2 are the stresses that represent the self-weight of the upper portion of the pile and the overlying soil stratum, respectively (b) view of the DEM[3D] models of rock sockets with different roughness RF values.

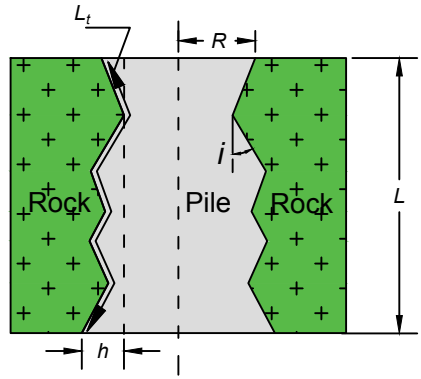

Fig. 7. Parameters for defining the roughness factor (modified from Zhang 2004).

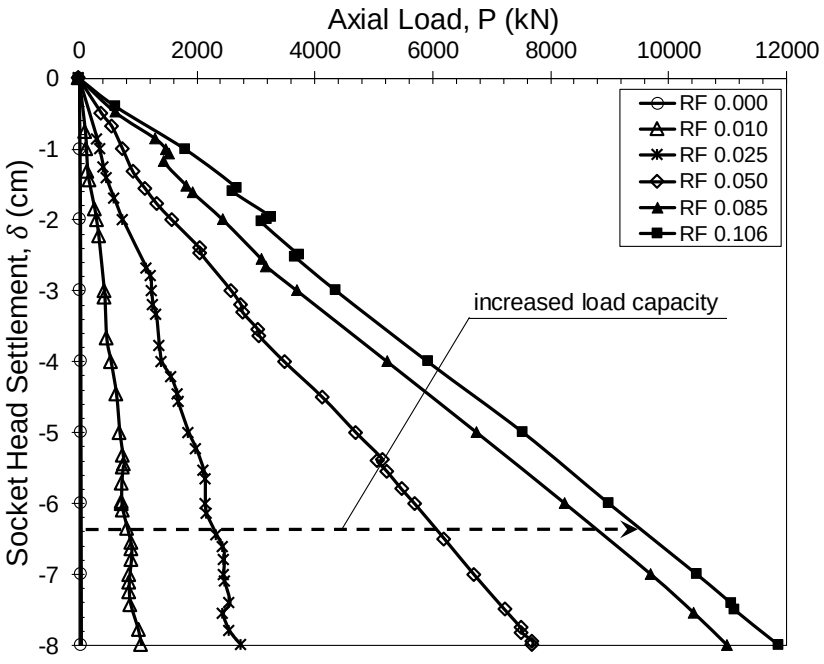

Fig. 8. Comparison of load-settlement responses of rock-socketed piles on sandstone-S3 with different roughness computed with DEM^{3D} models.

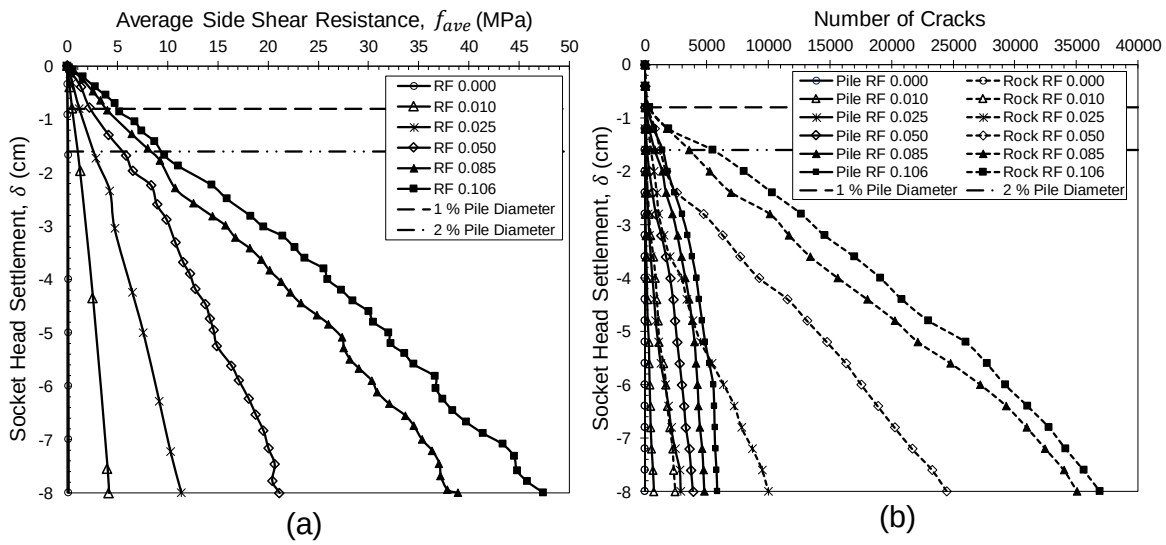

Fig. 9. (a) average side shear resistance (f_{ave}) versus socket head settlement (δ) on sandstone-S3, (b) number of cracks versus socket head settlement (δ) on sandstone-S3.

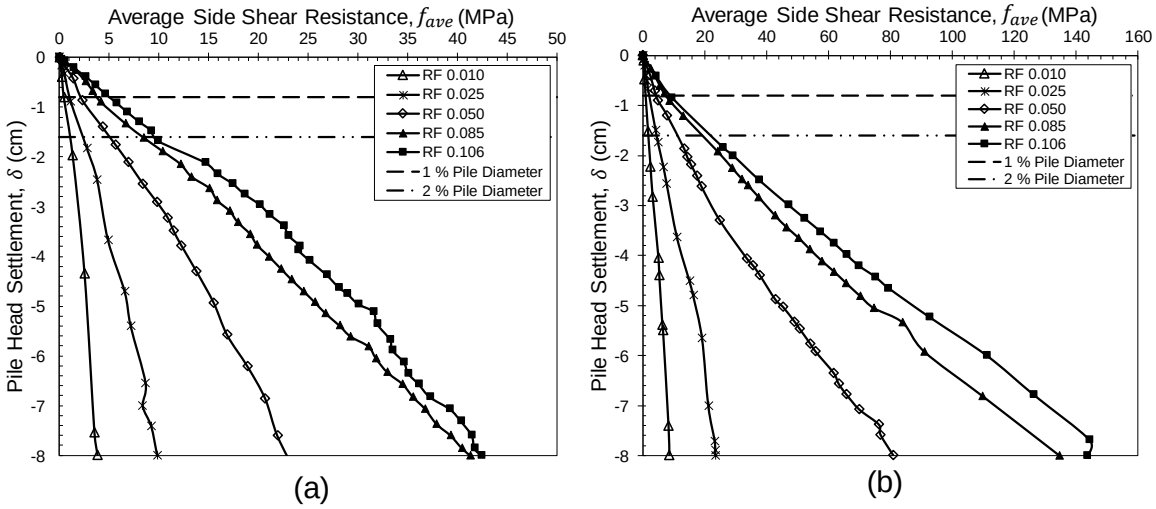

Fig. 10. Average side shear resistance (f_{ave}) versus socket head settlement (δ) on (a) sandstone-S2, (b) gneiss.

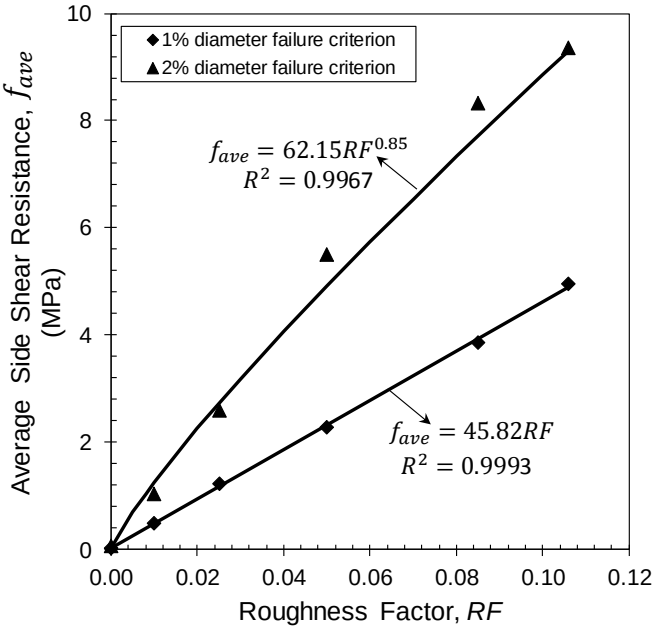

Fig. 11. Average side shear resistance (f_{ave}) versus roughness factor (RF) for a pile head movement equivalent to 1% and 2% of the pile diameter on sandstone-S3 computed with DEM^{3D} numerical models.

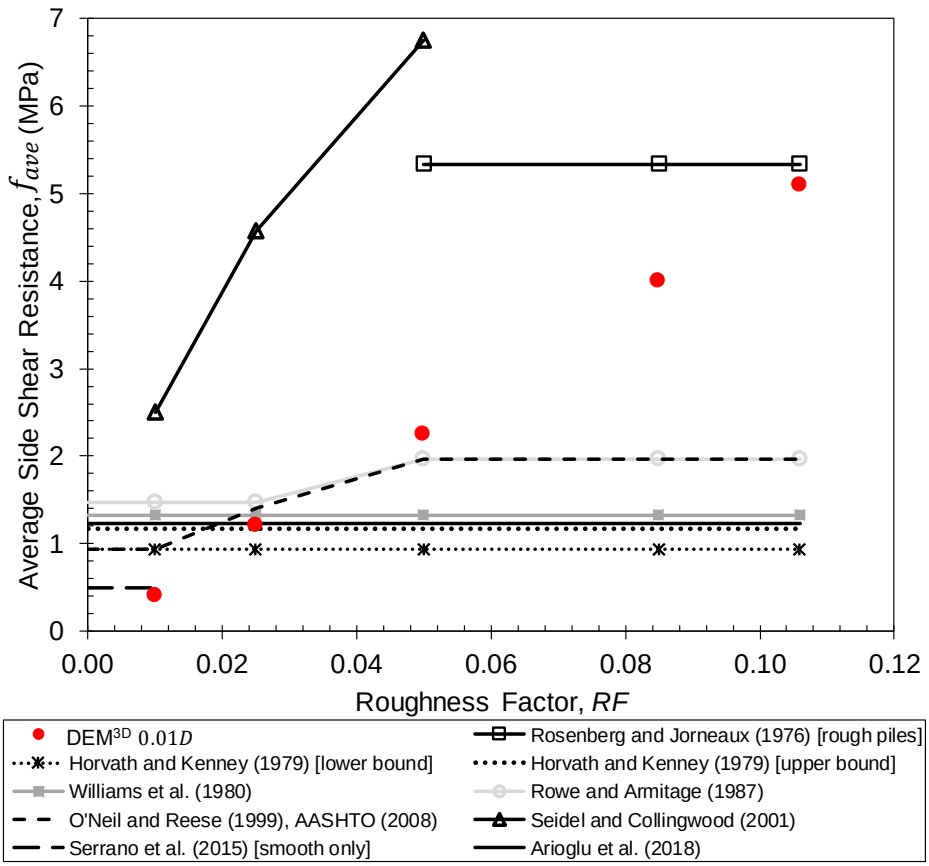

Fig. 12. Side shear resistance estimation: comparative between DEM^{3D} results (on sandston-S3) and empirical and analytical criteria.

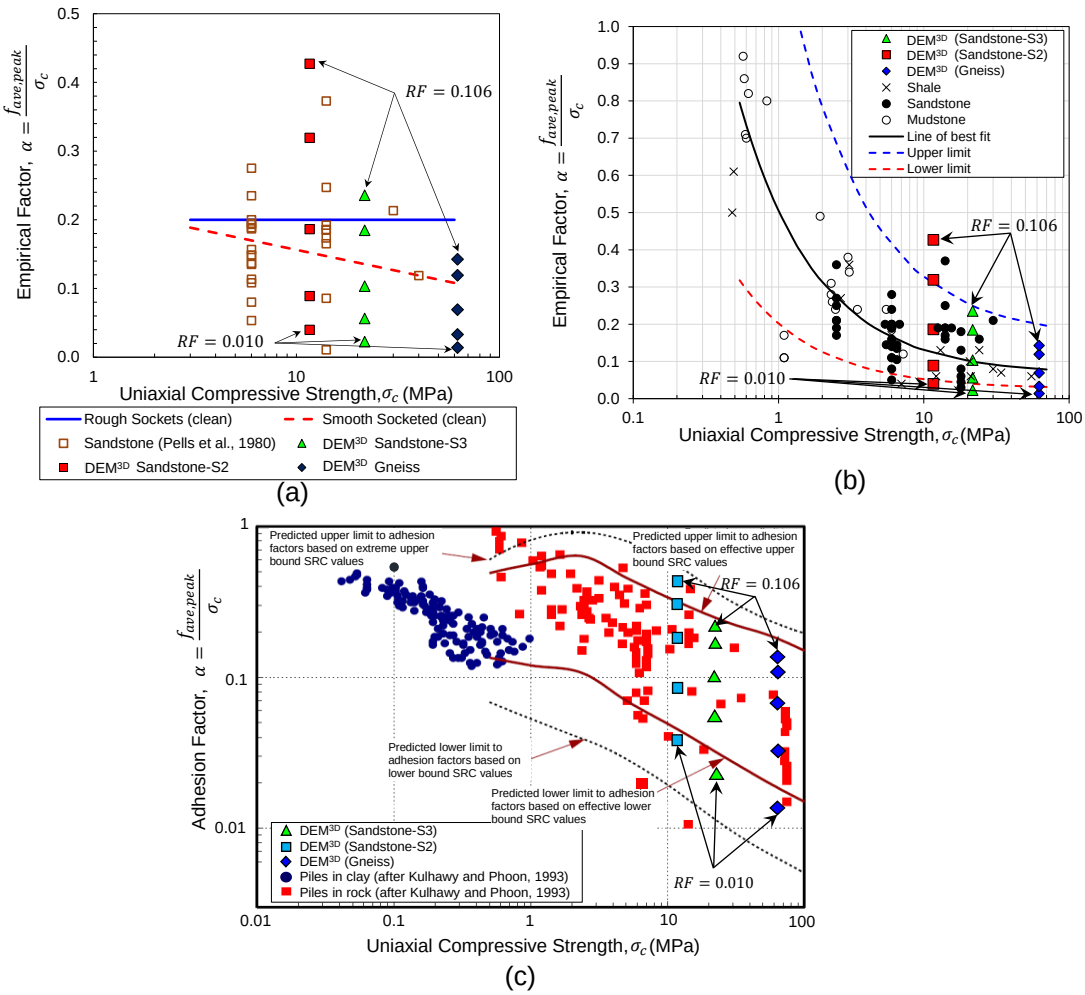

Fig. 13. DEM[3D] results compared with design curves proposed (a) by Pells et al. (1980), (b) by Williams and Pells (1981), (c) by Seidel and Collingwood (2001) after incorporated the load tests data of Kulhawy and Phoon (1993).